Minimally parametric power spectrum reconstruction from the Lyman α forest

Simeon Bird,[1*] Hiranya V. Peiris,[1,2] Matteo Viel[3,4] and Licia Verde[5]

[1]*Institute of Astronomy and Kavli Institute for Cosmology, Madingley Road, Cambridge CB3 0HA*
[2]*Department of Physics and Astronomy, University College London, London WC1E 6BT*
[3]*INAF - Osservatorio Astronomico di Trieste, Via G.B. Tiepolo 11, I-34131 Trieste, Italy*
[4]*INFN/National Institute for Nuclear Physics, Via Valerio 2, I-34127 Trieste, Italy*
[5]*ICREA & Instituto de Ciencias del Cosmos, Universitat de Barcelona, Marti i Franques 1, 08028 Barcelona, Spain*

ABSTRACT

Current results from the Lyman α forest assume that the primordial power spectrum of density perturbations follows a simple power-law form. We present the first analysis of Lyman α data to study the effect of relaxing this strong assumption on primordial and astrophysical constraints. We perform a large suite of numerical simulations, using them to calibrate a minimally parametric framework for describing the power spectrum. Combined with cross-validation, a statistical technique which prevents overfitting of the data, this framework allows us to reconstruct the power spectrum shape without strong prior assumptions. We find no evidence for deviation from scale-invariance; our analysis also shows that current Lyman α data do not have sufficient statistical power to robustly probe the shape of the power spectrum at these scales. In contrast, the ongoing Baryon Oscillation Sky Survey will be able to do so with high precision. Furthermore, this near-future data will be able to break degeneracies between the power spectrum shape and astrophysical parameters.

Key words: methods: numerical – methods: statistical – intergalactic medium – cosmology: theory.

1 INTRODUCTION

The primordial power spectrum of density fluctuations underpins much of modern cosmology. On large scales, it has been measured with high precision by cosmic microwave background (CMB) experiments (e.g. Komatsu et al. 2011 and references within). In order to improve our knowledge of its scale-dependence, we turn to smaller scales, and astrophysical measurements probing later epochs in the evolution of the Universe. In this paper, we shall examine constraints from the data set which has probed the smallest scales to date: the Lyman α forest.

The Lyman α forest consists of a series of features in quasar spectra due to scattering of quasar photons with neutral hydrogen. Since hydrogen makes up most of the baryonic density of the Universe, the Lyman α forest traces the intergalactic medium (IGM), and thus the baryonic power spectrum, on scales from a few up to tens of Mpc. This makes it the only currently available probe of fluctuations at small scales in a regime when the corresponding density fluctuations were still only mildly non-linear, thereby simplifying cosmological inferences. A number of authors have examined the cosmological constraints from the Lyman α forest in the past (Croft

et al. 1998; Theuns et al. 1998; McDonald et al. 2000; Hui et al. 2001; Viel et al. 2002; Gnedin & Hamilton 2002; McDonald et al. 2005b; Lidz et al. 2006; Viel & Haehnelt 2006), while Seljak et al. (2005) and Seljak, Slosar & McDonald (2006) examined constraints combined with other data sets. For a review of the physics of the IGM and its potential for cosmology, see Meiksin (2009).

Previous analyses assumed that the primordial power spectrum on Lyman α scales is described by a nearly scale-invariant power law – a strong prior – and proceeded with parameter estimation under this assumption. In contrast, in this work we attempt to constrain the shape and amplitude of the primordial power spectrum at these scales using minimal prior assumptions about its scale-dependence.

In view of the observational effort dedicated to the Lyman α forest, and its promise as a probe of the primordial power spectrum, in this work we shall explore the possibilities of going beyond parameter fitting. To give us insight into the underlying model for the power spectrum shape, which parameter estimation by itself cannot do, our present application to Lyman α data should therefore ideally assume full shape freedom throughout the analysis. As a nearly scale-invariant primordial power spectrum is a generic prediction of the simplest models of inflation, a minimally parametric reconstruction can be a powerful test of inflationary models. Lyman α constrains the smallest cosmological scales; thus, it provides the longest lever-arm when combined with the statistical power and

---

*E-mail: spb41@ast.cam.ac.uk

robustness of CMB data, yielding the best opportunity presently available to understand the overall shape of the power spectrum.

The main Lyman α observable, the flux power spectrum, does not have a simple algebraic relationship to the matter power spectrum. By $z \sim 3$, the absorbing structures are weakly non-linear, and are also affected by baryonic physics. Hence, to establish the relationship between the primordial power spectrum and the flux power spectrum, we must resort to hydrodynamical simulations. The initial conditions used in our simulations allow for considerable freedom in the shape of the primordial power spectrum, and this allows us to recreate the Lyman α forest resulting from generic power spectrum shapes. Using an ensemble of simulations which sample the parameter space required to describe the flux power spectrum, we construct a likelihood function which can be used to perform minimally parametric reconstruction of the primordial power spectrum, while simultaneously constraining parameters describing IGM physics.

A statistical technique called cross-validation (CV) is used to robustly reconstruct the primordial power spectrum and Markov Chain Monte Carlo (MCMC) techniques are used to obtain the final constraints. The statistical approach parallels Sealfon, Verde & Jimenez (2005) and Verde & Peiris (2008), who applied the same method to data from the CMB and galaxy surveys. Peiris & Verde (2010) added the current Lyman α forest data to the joint analysis with larger scale data, via the derived constraints on the small-scale matter power spectrum from McDonald et al. (2005b). However, these latter constraints were derived assuming a tight prior on the shape of the primordial power spectrum at Lyman α scales – an assumption which we drop in this work. In our analysis, we consider both the flux power spectrum determined by McDonald et al. (2006) from low-resolution quasar spectra obtained during the Sloan Digital Sky Survey (SDSS), and simulated data for the upcoming Baryon Oscillation Sky Survey (BOSS: Schlegel, White & Eisenstein 2009).

This paper is organized as follows. In Section 2 we review the framework for power spectrum reconstruction and describe the details of the simulations and parameter estimation setup. Section 3 describes the data, and results are presented in Section 4. We conclude in Section 5. Technical details of our calculations are relegated to Appendices A and B.

2 METHODS

In this section, we describe the statistical technique used in this paper, and how we built the likelihood function for minimally parametric reconstruction from Lyman α data. Section 2.1 describes the framework for power spectrum reconstruction in general terms, while Section 2.2 gives further details of our specific implementation of this framework. Sections 2.3–2.5 detail numerical methods used to extract a flux power spectrum from a given primordial power spectrum. Finally, Section 2.6 describes the parameter estimation implementation.

2.1 Power spectrum reconstruction

Previous analyses of the Lyman α forest (Viel, Haehnelt & Springel 2004; McDonald et al. 2005b) have assumed that the primordial power spectrum is a nearly scale-invariant power law of the form

$$P(k) = A_s \left(\frac{k}{k_0}\right)^{n_s - 1 + \alpha_s \ln k}, \tag{1}$$

and then constrained A_s, n_s and α_s. In this work we will follow the same spirit as Sealfon et al. (2005) and Verde & Peiris (2008), going beyond parameter estimation in an attempt to deduce what the Lyman α forest data can tell us about the shape of the power spectrum under minimal prior assumptions. A major challenge involved in all such reconstructions is to avoid overfitting the data; it is of little use to produce a complex function that fits the data set extremely well if we are simply fitting statistical noise. Equally, an overly prescriptive function which is a poor fit to the data should be rejected. To achieve this balance, we add an extra term, $\mathcal{L}_P$, to the likelihood function which penalizes superfluous fluctuations. Schematically, the likelihood function is

$$\log \mathcal{L} = \log \mathcal{L}[\text{Data}|P(k)] + \lambda \log \mathcal{L}_P, \tag{2}$$

where the form of $\mathcal{L}_P$ will be discussed shortly. Equation (2) now contains an extra free parameter which measures the magnitude of the smoothing required; the penalty weight λ. As $\lambda \to \infty$, the likelihood will implement linear regression. For particularly clean data, carrying no evidence for any feature in the $P(k)$, λ should be large. Data carrying strong evidence for $P(k)$ features would be best analysed with a small value of λ. We need a method of determining, from the data, the optimal penalty weight. Our chosen technique is called CV (Green & Silverman 1994), which quantifies the idea that a correct reconstruction of the underlying information should accurately predict new, independent data.

The variant of CV used in this paper splits the data into three sets. The function is reconstructed using two of these sets (training sets). The likelihood (excluding the penalty term) of this reconstruction, given only the data in the remaining set (validation set), is calculated. This step is called validation; because the data in each set are assumed to be independent, we now have a measure of the predictivity of the reconstruction. Validation is repeated using each set in turn and the total CV score is the sum of all three validation likelihoods. The optimal penalty is the one which maximizes the CV score.

More generally, CV splits the data into k independent sets, with $2 < k \leq n$, where n is the number of data points. $k - 1$ sets are used for training, and the remaining set for validation. Larger k allows for a bigger training set, and thus better estimation of the function to be validated against, but for most practical problems large k is computationally intractable. We have chosen $k = 3$ as a compromise. We verified that using $k = 2$, following Verde & Peiris (2008), made a negligible difference to our results despite the smaller training set size.

CV assumes that each set is uncorrelated; a mild violation of this assumption will lead to an underestimation of errors, but not a systematic bias in the derived parameters (Carmack et al. 2009). Our data include a full covariance matrix, and so we are able to verify that correlations between the sets are weak.

The minimally parametric framework applied in this paper follows that of Sealfon et al. (2005), Verde & Peiris (2008) and Peiris & Verde (2010). It uses cubic splines to reconstruct a function $f(x)$ from measurements at a series of points, x_i, called the knots. The function value between each pair of knots is interpolated using a piecewise cubic polynomial. The spline is fully specified by the knots, continuity of the first and second derivatives, and boundary conditions on the second derivatives at the exterior knots (the knots at either end of the spline). The splines have vanishing second derivative at the exterior knots. If the power spectrum is given by smoothed splines, the form of the likelihood function given above

Table 1. Positions of the knots. The maximum and minimum values of $P(k)$ are the extremal values covered by our simulations. Fixed knots are not shown, but are discussed in the text.

Knot	Position (Mpc^{-1})	$P(k)$ ($/10^{-9}$)	
		Minimum	Maximum
A	0.475	0.83	3.25
B	0.75	0.60	3.23
C	1.19	0.60	3.67
D	1.89	0.53	4.16

is

$$\log \mathcal{L} = \log \mathcal{L}[\mathrm{Data}|P(k)] + \lambda \int_k \mathrm{d}\ln k\,[P''(k)]^2,$$

$$\text{where } P''(k) = \frac{\mathrm{d}^2 P}{\mathrm{d}(\ln k)^2}. \tag{3}$$

2.2 Knot placement

The number and placement of the knots is chosen initially and kept fixed throughout the analysis. Once there are sufficient knots to allow a good fit to the data, adding more will not alter the shape of the reconstructed function significantly. In choosing the number of knots, we seek to find a balance between allowing sufficient freedom in the power spectrum and having few enough parameters that the data are still able to provide meaningful constraints on two sets out of three when subdividing the data into the training and validation sets, as described above. Available computing resources limit us in any case to considering only a few knots. We fit the primordial power spectrum with a four-knot spline for the Lyman α forest k-range. The flux power spectrum is available in 12 k-bins, so there are three bins per knot, which should allow sufficient freedom. By comparison, Peiris & Verde (2010) used seven knots to cover the k-range spanned by CMB, galaxy surveys and Lyman α data, with a single knot for the Lyman α forest.

The SDSS flux power spectrum covers the range of scales, in velocity units, of $k_v = 1.41 \times 10^{-3} - 0.018\,\mathrm{s\,km^{-1}}$. Dividing by a factor of $H(z)/(1 + z)$ converts to comoving distance coordinates, so the constraints on the matter power spectrum are on scales of roughly $k = 0.4$–$3\,\mathrm{Mpc^{-1}}$. In this range of scales, we place four knots (A–D, from large to small scales) evenly in log space. Numerical details of the knots are shown in Table 1. The maximum and minimum values of $P(k)$ given there for each knot are simply the extremal values covered by our simulations. Simulation coverage of $P(k)$ has been expanded where necessary, to fully cover the range allowed by the data.

We must specify the primordial power spectrum on scales well outside the range probed by data, even though they have no effect on the Lyman α forest. This is for two reasons. The first is that when running a simulation we must have a well-defined way to perturb the initial particle grid for all scales included in the simulation. In order to ensure that the scales on which we have data are properly resolved, we also need to simulate larger and smaller scales, and these require a defined power spectrum. The second reason is that our interpolation scheme works best when the perturbations induced by altering one of the knots are reasonably local. Adding extra end knots helps to prevent large secondary boundary effects, which would make interpolation far more difficult.

For numerical stability reasons, we would like the amplitude of fluctuations on these scales to be reasonably constant, but do not wish to make strong assumptions about the amplitude of the power
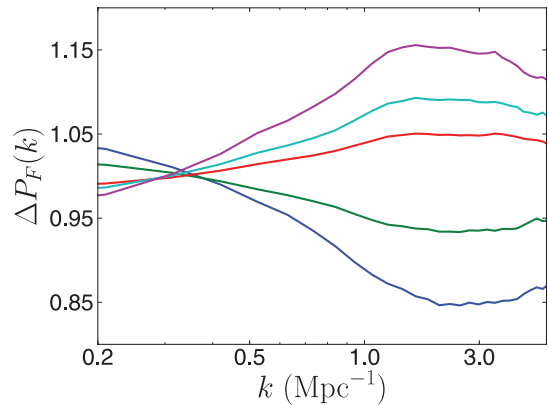

Figure 1. Effect on the flux power spectrum of varying the D knot at $z = 3$. On a scale where the best-fitting amplitude is 0.9, the amplitudes of the D knot are, from the lowest line upwards, 0.5, 0.7, 1.1, 1.3 and 1.7. Non-linear growth tends to erase dependence on the initial conditions, so the effect is smaller at lower redshifts.

spectrum there. Therefore we add two 'follower' knots at each end of the spline. The amplitude is fixed to follow the nearest parameter knot, assuming that between follower and followed, the shape is a power law with $n_s = 0.97$.[1] The two follower knots are at scales of $k = (0.15, 4)\,\mathrm{Mpc^{-1}}$.

We also add a few knots, even more distant from the scales probed by the data, with completely fixed amplitudes consistent with the *Wilkinson Microwave Anisotropy Probe* (*WMAP*) best-fitting power spectrum. The amplitude of the primordial power spectrum on these scales does not significantly affect results; we have added knots here so that the initial density field is well defined on a larger range of scales than probed by the simulation. This allows us to avoid any boundary effects associated with the ends of the spline. These fixed knots are at $k = (0.07, 25, 40)\,\mathrm{Mpc^{-1}}$, with amplitudes of $(2.43, 2.03, 2.01) \times 10^{-9}$. Fig. 1 shows the effect of altering the amplitude of the D knot on the flux power spectrum.

2.3 Simulations

In this study, full hydrodynamical simulations were run using the parallel TreePM code GADGET-2 (Springel 2005). GADGET computes long-range gravitational forces using a particle grid, while the short-range physics are calculated using smoothed particle hydrodynamics (SPH), where particles are supposed to approximate density elements in the matter fluid. Hydrodynamical effects are included by having two separate particle types: dark matter, affected only by gravity, and baryons, affected also by pressure forces and other baryonic physics. The rest of this section gives technical details of our simulations and the included astrophysics, and may be skipped by the reader interested only in the cosmological implications.

GADGET has been modified to compute the ionization state of the gas using radiative cooling and ionization physics as originally described by Katz, Weinberg & Hernquist (1996) and used in Viel & Haehnelt (2006). Star formation is included via a simplified prescription which greatly increases the speed of the simulations, where all baryonic particles with overdensity $\rho/\rho_0 > 10^3$ and temperature $T < 10^5\,\mathrm{K}$ are immediately made collisionless. Viel et al. (2004)

---

[1] Hence, if the amplitude of the power spectrum at the D knot is P^D, the power spectrum at the follower knot has the amplitude $P^D(k^D/k^{D+1})^{0.03}$, where k^D is the position of the D knot and k^{D+1} the position of the follower.

compared simulations using this prescription with identical simulations using a multiphase model, and found negligible difference in the Lyman α statistics. Additionally, all feedback options have been disabled and galactic winds neglected; Bolton et al. (2008) found that winds have a small effect on the Lyman α forest. The gravitational softening length was set to 1/30 of the mean linear interparticle spacing.

The gas is assumed to be ionized by an externally specified, spatially homogeneous UV background, based on the galaxy and quasar emission model of Haardt & Madau (2001). We follow previous analyses in assuming that the gas temperature is initially in equilibrium with the CMB, that the gas is in ionization equilibrium, optically thin, and that we can neglect metals and evolution of elemental abundances. Lyman α absorption arises largely from near mean-density hydrogen, which should undergo little chemical evolution, so using a simplified star formation criterion and neglecting metals is physically well motivated. Assuming that the gas is optically thin and in ionization equilibrium will break down during reionization, but at the redshifts we are interested in, we can model the effect of non-instantaneous reionization by increasing the photoheating rate, as described in Viel & Haehnelt (2006).

The fiducial simulation for this paper has a box size of 60 Mpc h^{-1} and 2×400^3 gas and dark matter particles, [which we will write as (60, 400) in future], and runs from $z = 199$ to 2. Snapshots are output at regular intervals between redshift 4.2 and 2.0. Initial conditions were generated using N-GenICs, modified to specify the primordial power spectrum by a spline, and use separate transfer functions for baryons and dark matter, as calculated using CAMB (Lewis, Challinor & Lasenby 2000).

For knots B and C, we used the above fiducial parameters for box size and particle resolution. For the D knot, we slightly compromised on box size in favour of particle resolution, and used simulations of (48, 400), since we found that the D knot had a negligible affect on the largest scales. To fully capture the behaviour of the A knot, we used larger simulations with (120, 400). We have used different sized simulations to ensure that for each knot, the characteristic scales representing it have very good numerical convergence; this issue is addressed in full in Appendix B. Our ability to do this is one technical advantage of our approach compared with previous studies; if we were to alter the amplitude of the whole power spectrum, we would need to achieve convergence over all the relevant scales at once. In our approach, each simulation only needs strict convergence over the narrow range of scales probed by a single knot.

2.4 IGM thermodynamics

Constraints on the thermal history of the IGM are given in terms of the parameters of a polytropic temperature–density relation:

$$T = T_0 \left(\frac{\rho}{\rho_0}\right)^{\gamma - 1}, \tag{4}$$

where a given SPH particle has temperature T and density ρ. T_0 and ρ_0 are the average quantities for the whole simulation snapshot. To determine T_0 and γ from a simulation box, a least-squares fit is performed from low-density particles satisfying

$$-1.0 < \log\left(\frac{\rho}{\rho_0}\right) < 0. \tag{5}$$

Regions that are less dense than the lower limit above are ignored because they are poorly resolved in SPH simulations (Bolton & Becker 2009). The simplified star formation criterion means that

many overdensities have been turned into stars, and their baryonic evolution not followed; hence they are also neglected. Both γ and T_0 are assumed to follow a power law broken at $z = 3$ by He II reionization (Schaye et al. 2000), so that they are given by

$$\gamma = \begin{cases} \gamma^A \left[(1+z)/4\right]^{d\gamma^S} & \text{if } z < 3, \\ \gamma^A \left[(1+z)/4\right]^{d\gamma^R} & \text{if } z > 3. \end{cases} \tag{6}$$

$$T_0 = \begin{cases} T_0^A \left[(1+z)/4\right]^{dT_0^S} & \text{if } z < 3, \\ T_0^A \left[(1+z)/4\right]^{dT_0^R} & \text{if } z > 3. \end{cases} \tag{7}$$

When performing parameter estimation, we marginalize over γ^A, T_0^A and $d\gamma^{S,R}$, $dT_0^{S,R}$. The different thermal histories were constructed by modifying the fiducial simulation's photoheating rate as described in section 2.2 of Bolton et al. (2008).

The effective optical depth is described by a power law, with parameters:

$$\tau_{\text{eff}} = \tau_{\text{eff}}^A \left[(1+z)/4\right]^{\tau_{\text{eff}}^S}. \tag{8}$$

Previous studies (McDonald et al. 2005b; Viel & Haehnelt 2006) used the same transfer function for both dark matter and baryon particles; we have used different transfer functions for baryon and dark matter species. At our starting redshifts, the transfer functions for the baryons are about 10 per cent lower than for the dark matter on these scales, because baryon fluctuations have not grown as fast during tight coupling. Once they have decoupled from the photons, the baryons fall into the potential wells of the dark matter, and by $z = 1$, the linear transfer functions are almost identical. At redshifts 2–3, however, the effect is small but noticeable, and accounts for a 2 per cent scale-independent drop in the power spectrum. This is too small to affect current data, but could be potentially important for analysing BOSS data.

2.5 The flux power spectrum

In the case of Lyman α, the observable is not a direct measurement of the clustering properties of tracer objects, as in galaxy clustering, but the statistics of absorption along a number of quasar sightlines. Therefore we define the flux, $\mathcal{F}$, as

$$\mathcal{F} = \exp(-\tau), \tag{9}$$

where τ is the optical depth. We define the flux power spectrum as

$$P_F(k) = |\tilde{\delta}_F(k)|^2,$$
$$\delta_F = \frac{\mathcal{F}}{\bar{\mathcal{F}}} - 1. \tag{10}$$

Here $\bar{\mathcal{F}}$ is the mean flux. The tilde denotes a Fourier transformed quantity, where our Fourier conventions, used throughout, are

$$\tilde{f}(k) = \int f(x) e^{ikx} dx. \tag{11}$$

To aid the eventual understanding of our results, we digress slightly here to review the physical effects of the various thermal parameters on the flux power spectrum. The mean flux, essentially a measure of the average density of neutral hydrogen, has a large impact on the amplitude of the flux power spectrum. Cosmological information from the Lyman α forest is obtained through examining the power spectrum shape and its redshift dependence. The effect of a higher temperature, as preferred by the flux power spectrum, is to suppress power predominantly on small scales, as a higher temperature wipes out small-scale structure in the baryons. The exponent

of the temperature–density relation, γ, controls the temperature difference between voids and overdensities. A higher γ makes voids cooler and overdensities hotter. At high redshifts, where much of the Lyman α absorption comes from voids, the effect of an increased γ is to decrease the temperature of the Lyman α emitting regions, so there is relatively more small-scale structure. At low redshifts, however, most of the Lyman α absorption comes from near mean-density material, and so an increased γ increases the temperature, decreasing the amount of small-scale structure. For further details of the physical effects of the various parameters, see Section 4.2.1 and fig. 3 of Viel & Haehnelt (2006), as well as figs 11–13 of McDonald et al. (2005b).

Current constraints on P_F are given by McDonald et al. (2006), determined from ~3000 SDSS quasar spectra at $z = 2$–4.

Each simulation snapshot was processed to generate an averaged flux power spectrum as follows. First, 8000 randomly placed simulated quasar sightlines were drawn through the simulation box. For a $60\,\mathrm{Mpc}\,h^{-1}$ box, this constitutes an average spacing between sightlines of $670\,h^{-1}\,\mathrm{kpc}$, corresponding to scales of roughly $k = 10\,\mathrm{Mpc}\,h^{-1}$, far smaller than the scales probed by the Lyman α forest. We verified that doubling the number of sightlines to 16 000 made a negligible difference to the resulting power spectra.

When calculating absorption, particle peculiar velocities were included, which increases the (non-rescaled) magnitude of the power spectrum by approximately 10 per cent.

To generate the flux power spectrum, the absorption due to each SPH particle near the sightline is calculated, giving us a number of simulated quasar spectra, which are smoothed with a simple boxcar average. Each spectrum is rescaled by a constant so that the mean flux across all spectra and absorption bins matches that observed by Kim et al. (2007). This rescaling hides our ignorance of the amplitude of the photo-ionizing UV background. The mean over all the rescaled spectra is then used as the extracted flux power spectrum for the box. For further details of how we computed the absorption, see Appendix A.

We follow previous work in not attempting to model continuum fitting errors. The Si III contamination found by McDonald et al. (2006) is modelled by assuming a linear bias correction of the form $P_F' = [(1 + a^2) + 2a \cos(vk)]P_F$, with $a = f_{\mathrm{Si\,III}}/(1 - \bar{\mathcal{F}})$, $f_{\mathrm{Si\,III}} = 0.011$ and $v = 2271\,\mathrm{km\,s^{-1}}$.

Finally, since high-density, damped Lyman α systems (DLAs) are not modelled by our simulations, we add a correction to the flux power spectrum to account for them, of the form calculated by McDonald et al. (2005a). The amplitude of this correction is a free parameter, and will be discussed further in Section 2.6.2.

We checked the convergence of our simulations with respect to box size and particle resolution. Here we give only a brief summary of the results; further details may be found in Appendix B. For the highest redshift bins at $z = 4.2$, 4.0 and 3.8, increasing the particle resolution had a large effect on the flux power spectrum. Achieving numerical convergence for the Lyman α forest at high redshift is challenging, because most of the signal for the Lyman α forest is coming from poorly resolved underdense regions. In addition, current data at high redshifts are much more noisy than at low redshifts, and future surveys will not probe these redshifts at all. Accordingly, we follow Viel & Haehnelt (2006) and do not use the three highest redshift bins in our analysis.

At lower redshifts, and except in the smallest and largest k-bins, the change with increased particle resolution was small. On the smallest scales, however, there was a change of around 5 per cent in each bin. This increase is systematic, and so we correct for it as described in Appendix B. The larger box increased power on the

largest scales by around 5 per cent, due to sample variance in the simulation box. The methodology we used to correct for this effect is again detailed in Appendix B.

The above figures were the dominant errors in our modelling of the flux power spectrum. Uncorrected modelling errors are therefore $\lesssim 2$ per cent of the flux power spectrum in each bin, far below the current measurement error of ~12 per cent in each bin of the flux power spectrum, and on the order of the expected statistical errors for the BOSS survey, which are ~1.5 per cent. A significant decrease in modelling errors would require the use of simulations with improved particle resolution, which are beyond the computational resources available to us.

2.6 Parameter estimation

So far we have given a formula for the primordial power spectrum, and described how we use it to extract a flux power spectrum to compare with observational data. In this section, we shall describe how we actually performed that comparison. First we describe a scheme for robustly interpolating the parameter space to obtain flux power spectra corresponding to parameter combinations which we have not simulated, following Viel & Haehnelt (2006). Secondly, we describe the parameters of the Monte Carlo Markov Chains (MCMCs) we used for parameter estimation. For more details of MCMC, see for example Lewis & Bridle (2002).

2.6.1 Parameter interpolation

Directly calculating a flux power spectrum from a given set of primordial fluctuations requires a hydrodynamical simulation. This makes it impractical to directly calculate P_F for every possible set of input parameters. Instead, simulations are run for a representative sample and other results are obtained from these via interpolation. We assume that the flux power spectrum varies smoothly around the best-guess model, parametrizes this variation with a quadratic polynomial for each data point and then check that this accurately predicts new points. If we have some simulation with a parameter vector which differs from a 'best-guess' simulation by δp_i, the corresponding change in the flux power spectrum, δP_F, is given by

$$\delta P_F = \sum_j \alpha_j \delta p_j + \beta_j \delta p_j^2. \tag{12}$$

The coefficients of this polynomial are constrained by performing a least-squares fit to flux power spectra generated by numerical simulations. We experimented with including cross-terms (of the form $p_i p_j$), but found that this did not significantly improve the accuracy of the interpolation.

To estimate the interpolation coefficients, we used seven simulations for each of our four power spectrum parameters, one of which was used to test the accuracy of the interpolation. To check for correlation between parameters, we simulated varying two neighbouring knots at once. As the greatest effect of each knot on the flux power spectrum is over a localized range of scales, our interpolation errors should be maximal here. We needed only four simulations per thermal history parameter, and checked we could accurately predict δP_F for a very different thermal history. As a final interpolation verification, we performed a simulation where all six parameters were changed simultaneously. Fig. 2 shows the interpolation errors for one of our tests, which are around 1 per cent of the total change for each bin. This is smaller than the expected statistical errors for BOSS, and was replicated by our other test simulations.
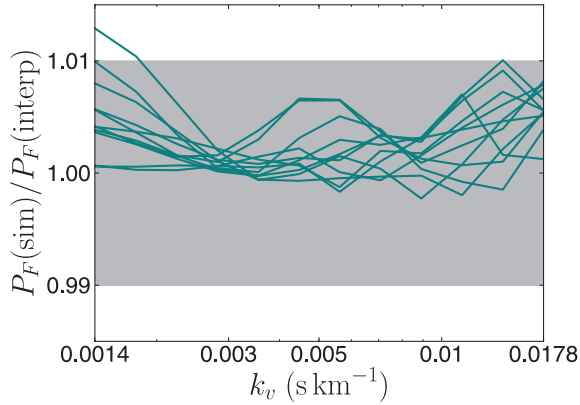
Figure 2. The difference between the flux power spectrum as obtained from interpolation, and directly by simulation. Here only the C and D knots have been changed from their initial values. Each line represents simulation output at a different redshift bin, between $z = 2.0$ and 4.2. The grey band shows 1 per cent error bars.

2.6.2 MCMC methodology

To perform parameter estimation, we use a version of the publicly available CosmoMC (Lewis & Bridle 2002) code, with a modified likelihood function as described in Section 2.1.

We marginalize over four parameters for the four knots, with priors as specified in Table 1, and over eight parameters of the thermal history, as described in Section 2.3.

We follow the advice of McDonald et al. (2006), and add a number of nuisance parameters to the SDSS data, all with Gaussian priors. To parametrize uncertainty in the resolution of the spectra, we add a parameter α^2 with prior 0 ± 49, and multiply the flux power spectrum by $\exp(-k^2\alpha^2)$. The effect of an increased α^2 is therefore to damp power on the very smallest scales. Each redshift bin has one parameter, f_i, to describe uncertainty in the subtraction of background noise, with a prior of 0 ± 0.05. To marginalize over the uncertainty in the effect of DLAs, we add A_{damp}, with a prior of 1 ± 0.3. The effect of this correction is to increase the slope of the flux power spectrum.

We also marginalize over residual uncertainties in the Hubble parameter, h and Ω_M, using flat priors of $0.2 < \Omega_M < 0.4$ and $0.5 < h < 0.9$. For the rest of our background cosmology, we assume parameters in agreement with those preferred by *WMAP* 7, including negligible gravitational waves and spatial curvature. The priors on h and Ω_M make a negligible difference to our results, because both these parameters only weakly affect the Lyman α forest. We assume $T_0 < 50\,000\,$K and $0 < \gamma < 5/3$ on physical grounds; the temperature–density relation of the IGM cannot be steeper than the perfect gas law, and very high temperatures would contradict independent measurements of the IGM temperature by Schaye et al. (2000).

2.6.3 Cross-validation methodology

CV requires the splitting of the data set into n independent sets. For best results, these sets should be as uncorrelated as possible. We choose to use alternating bins in k for each set. For data with n k bins, the first set would consist of bins 1, 4, 7. . ., the second bins 2, 5, 6. . . and the third similarly.

To calculate the CV score, we estimate the best fit from the two training sets, using an MCMC. The CV score for the remaining, validation, set is the likelihood of this best fit. The total CV score for a given penalty is the sum of the CV scores for each set.

3 DATA SETS

3.1 Current data from SDSS

The SDSS data used in this study consist of a best-fitting flux power spectrum in 12 k-bins and 11 redshift bins, together with a covariance matrix and a set of vectors describing the foreground noise subtraction. It was analysed by McDonald et al. (2006), and comes from 3000 quasar spectra. Of these, ~2000 are at redshift 2.2–3, and ~1000 above that. We use the eight redshift bins at $z <$ 3.8 only.

We have chosen not to include any additional small-scale information based on high-resolution quasar spectra. In principle, this can help break degeneracies and should be included in future analyses. Currently, however, systematic error from such data sets is hard to quantify, and the optimal method for extracting the thermal state of the IGM is not yet clear. Our focus in this work has been robustness, and so we have limited ourselves to a single data set, whose properties have been extensively studied and are relatively well understood.

3.2 Simulated data from BOSS

In this section we will describe our simulated data for forecasting constraints from BOSS, an ongoing future survey which will acquire 1.6×10^5 quasar spectra (Schlegel et al. 2009) between $z = 2.2$ and 3.0. We need to simulate both a covariance matrix and a flux power spectrum.

We have assumed that the noise per spectrum of the BOSS data will be approximately the same as they were for SDSS. This is a simple assumption, but broadly justified because both surveys use similar instruments (Schlegel et al. 2009). Truly accurate modelling of the covariance matrix is impossible until the release of the final data, however we expect our modelling of the BOSS covariance matrix to be completely adequate for a forecast. Our simulated BOSS covariance matrix is simply the SDSS covariance matrix scaled to account for the increase in statistical power resulting from the much greater number of quasar sightlines. There are roughly 2000 quasar sightlines in the SDSS sample below $z = 3$, so the scale factor is $2000/16\,0000 = 1/80$.

To generate the flux power spectrum, we used cosmological parameters consistent with the best-fitting results from *WMAP* 7, and thermal parameters consistent with theoretical expectations: $\gamma \sim$ 1.45 and $T_0 = 2.3 \times 10^3 [(1 + z)/4]^{0.2}$ K. The effective optical depth was $\tau = 0.36[(1 + z)/4]^{3.65}$. The power spectrum amplitude was selected to match a spectrum with $\sigma_8 = 0.8$ and $n_s = 0.96$.

We then added uncorrelated Gaussian noise with a variance given by the diagonal elements of the simulated BOSS covariance matrix. As BOSS will only take data at $z \leq 3$, we dispense with the thermal parameters for higher redshifts. The foreground noise properties of the BOSS data are expected to be similar to those of the SDSS data; we therefore leave the priors on the parameters measuring uncertainty in the noise subtraction and the parameter measuring resolution uncertainty, α^2, unchanged.

BOSS is also expected to determine the transverse flux power spectrum. Simulating the larger scales needed to properly model the effect of this is beyond the scope of this paper, and we refer the interested reader to Slosar et al. (2009) and White et al. (2010).
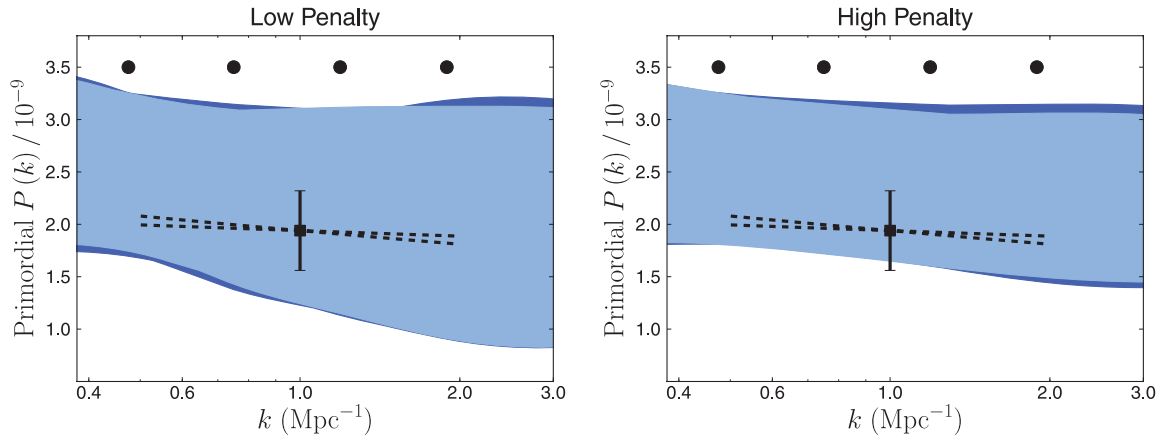
Figure 3. Constraints on the primordial power spectrum from SDSS data from CV, for low (left) and high (right) penalties. Black circles show the positions of the knots, with arbitrary normalization. The light blue regions show the top 68 per cent of likelihoods for SDSS data, while the dark blue regions show the 95 per cent likelihood range. The black error bar shows the results of previous analyses (Viel, Bolton & Haehnelt 2009) assuming a power-law power spectrum at $k = 1\,\mathrm{Mpc}^{-1}$. The dashed lines show limits on the slope from that work.

4 RESULTS

4.1 Current constraints

Fig. 3 shows the CV-reconstruction of the primordial power spectrum from SDSS data. We have emulated confidence limits by plotting the envelope of samples which have a likelihood in the top 68 per cent and the top 95 per cent. At the 95 per cent level, the power spectrum is allowed to oscillate more within the allowed envelope, but the size of the overall constraint on the amplitude does not greatly change, as found by Verde & Peiris (2008).

We have shown plots for two penalties: one high, one low. This was because we have been unable to determine an optimal penalty from current data; the CV score shows no significant variation, even when the penalty is having negligible impact on the likelihood. We interpret this to mean that the shape constraints on the primordial power spectrum from current Lyman α data are very weak.

Previous analyses assumed a power-law prior for the shape of the primordial power spectrum, and constrained this slope and the overall normalization from the same data used above. While such parameter estimation leads to tight constraints from the data (assuming the underlying shape prior is correct), relaxing this tight prior leads to the loss of ability to constrain the scale-dependent shape of the power spectrum. The current data can still be used as part of a minimally parametric primordial power spectrum if one exploits the extended range in scales that can be probed in combination with other data sets (Peiris & Verde 2010).

The black error bar in Fig. 3 shows a comparison with Viel et al. (2009). Our method gives results for the amplitude of the primordial power spectrum at Lyman α scales which are completely consistent with that work, but somewhat weaker. This is to be expected; we are removing a tight prior on the shape of the power spectrum. For a very high penalty, i.e. the limit at which the implicit prior in our analysis approaches a power-law spectrum, we can reproduce the error bars of Viel et al. (2009). We are also in agreement with the results of an earlier analysis of the Lyman α forest (McDonald et al. 2005b), which constrained $\sigma_8 = 0.85 \pm 0.13$.

The corresponding constraints on n_s from our reconstruction are extremely weak, especially for the low penalty: $n_s \sim 0.2$–1.2. The constraints on n_s in Seljak et al. (2005), in addition to the power-law prior, were greatly assisted by the fact that the pivot scale k_0 in
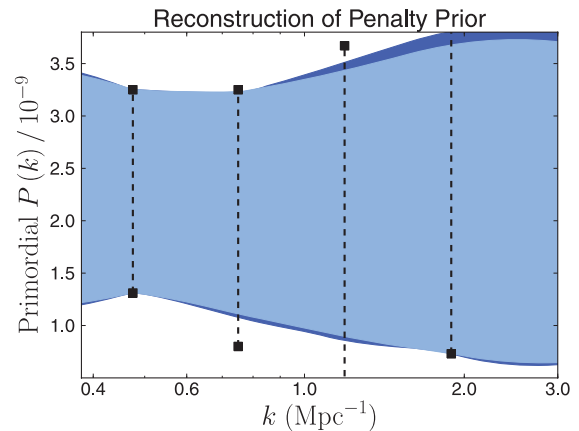

Figure 4. Constraints on the primordial power spectrum from the penalty term alone, using the value in the 'low penalty' plot of Fig. 3 above. Dashed lines show the power spectrum range sampled by the simulations.

equation (1) was chosen to be $k_0 = 0.002\,\mathrm{Mpc}^{-1}$; a small change in the slope of the power spectrum at k_0 leads to a large change in power spectrum amplitude by $k = 1\,\mathrm{Mpc}^{-1}$. Here, we are trying to constrain a scale-dependent $n_s(k) = 1 + (\mathrm{d}\ln P/\mathrm{d}\ln k)$ using only the interval of scales sampled by Lyman α forest. We find that, while the current Lyman α data are able to constrain the amplitude of the power spectrum at these scales, they are not powerful enough on their own to significantly constrain the shape of the spectrum in a robust manner. At no penalty do we see any evidence in the current data against a scale-invariant power spectrum.

We can explicitly demonstrate that the current Lyman α data add little information to a weak prior on the shape of the power spectrum in the following way. Fig. 4 shows a minimally parametric reconstruction assuming the penalty designated 'low'. These constraints were generated *without using any data whatsoever*, and are similar to those obtained with the Lyman α forest data. This figure shows clearly that our SDSS constraints are affected by the prior even for the low penalty. Since the penalty is proportional to $P''(k)$, it cannot determine the power spectrum amplitude. Instead, the allowed power spectrum amplitude is simply the minimal range probed by our simulations.

The CV part of our method involves reconstructing the optimal penalty, and thus the strength of the shape prior justified by the data. CV is essentially a method to reconstruct the most favoured prior correlation between knots; since the prior is reconstructed from the data, prior-driven constraints would not necessarily be a problem. However, here we are finding that no particular prior is favoured over any other. Thus, the width of the envelopes in Fig. 3 are actually arbitrary and should not be used to draw conclusions about the amplitude of primordial fluctuations at Lyman α scales.

We performed a number of checks to determine the cause of our failure to find an optimal penalty. Changing our methodology for splitting the data into CV bins did not affect the results. A flux power spectrum simulated in the same way as our BOSS data, and using the same parameters, but with error bars of the same magnitude as the current data showed no preference for a particular penalty, despite, as we shall see, there being a well-defined optimal penalty for BOSS simulations. Fixing the thermal history parameters γ and T_0 to fiducial values was also sufficient to allow us to reconstruct a penalty. Therefore, statistical error and systematic uncertainty in the thermal history are the significant factors preventing us from robustly reconstructing a minimally parametric power spectrum shape from current data.

Constraints on the thermal history parameters are as follows. For the low penalty we found $0.8 < \gamma < 1.7$ at 1σ (recall that this upper limit is imposed as a physical prior), while for the high penalty $0.2 < \gamma < 1.7$. The corresponding constraint from Viel et al. (2009) is $\gamma = 0.63 \pm 0.5$. There is a noticeable decrease in the best-fitting value of γ with an increased penalty (i.e. a stronger shape prior). We find it intriguing that we prefer an inverted temperature–density relation with $\gamma < 1.0$ only for a high penalty, but the constraints are so weak that we cannot draw any solid conclusions from them.

Constraints on the other parameters at 1σ were similar for both penalties. Those for the low penalty were $50000 > T_0 > 35000$ K, $\tau_{\mathrm{eff}} = 0.33 \pm 0.03$, a slope of $\tau_{\mathrm{eff}}^S = 3.3 \pm 0.3$, $h = 0.7 \pm 0.15$ and $\Omega_{\mathrm{M}} = 0.25 \pm 0.04$. Finally, constraints on the noise parameters largely reproduce the priors (listed in Section 2.6.2). Our results mirror those of Viel et al. (2009); we have therefore verified that those results are not biased by a shape prior on the power spectrum. The constraints of this work and Viel & Haehnelt (2006) on the IGM temperature, T_0, prefer a larger central value than that obtained by McDonald et al. (2005b). However, McDonald et al. (2005b) imposed a prior of $T_0 = 20\,000 \pm 2000$ K, derived from analysis of the flux probability distribution function of high-resolution quasar spectra, so a direct comparison is not possible. For further discussion of this intriguing result, we refer the interested reader to section 5 of Viel et al. (2009).

4.2 Simulated constraints from BOSS

Unlike current data, our simulated BOSS data show a well-defined maximum in the CV score. In Fig. 5 we show the constraints using this optimal penalty, together with our input power spectrum. The input data are reconstructed very well, within an envelope of roughly 0.4×10^{-9}; a precision comparable to that of a CV reconstruction from *WMAP* data (Verde & Peiris 2008). Even though our simulated power spectrum is nearly scale-invariant, we do not recover a very high optimal penalty. This is a feature of our approach; unless the data are noiseless, not all oscillations in the power spectrum will be ruled out, and the optimal penalty is one which allows for them while being consistent with experimental noise.

Our method was designed to extract $P(k)$, and so the penalty may not be entirely optimal for the derivative. Even given this, our
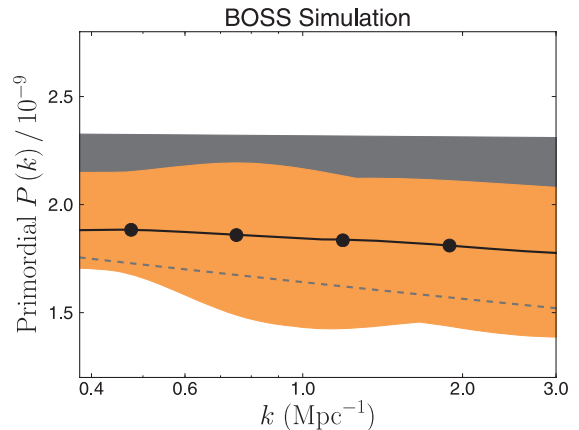

Figure 5. Constraints on the power spectrum for simulated BOSS data. Black circles show the positions of the knots, normalized to match the input power spectra (black line). The orange region shows the top 68 per cent of likelihoods from BOSS-quality Lyman α data. The grey region shows an extrapolation of the 1σ results from *WMAP* data to these scales, and the grey dashed line shows its lower extent.

constraints of $0.7 < n_s < 1.2$ are still comparatively weak. However, even this constraint could be useful to test for potential systematics, or in combination with other data sets. One other important data set will be the power spectrum of the cross-correlation of the flux (Viel et al. 2002; McDonald & Eisenstein 2007; Slosar et al. 2009), which BOSS is expected to measure for the first time. Estimating the power of combined constraints is beyond the scope of this paper, but it could be considerable.

Fig. 6 shows the thermal parameters as reconstructed from BOSS data. We have correctly reconstructed our input, as marked by the black dots. The reconstructed h and Ω_{M} were also consistent with their input values: $\Omega_{\mathrm{M}} = 0.27 \pm 0.02$ (input: 0.267), $h = 0.74 \pm 0.05$ (input: 0.72).

Marginalized constraints on the thermal and noise parameters are almost a factor of 2 better for BOSS than for current data. We have assessed the impact that further information about the thermal history of the IGM would have on cosmological constraints, imposing priors corresponding to present and reasonable near-future measurements:

$$\tau_{\mathrm{eff}} = 0.36 \pm 0.11, \qquad \tau_{\mathrm{eff}}^S = 3.65 \pm 0.25,$$
$$T_0 = 23000 \pm 3000 \,\mathrm{K}, \qquad \gamma = 1.45 \pm 0.2.$$

Constraints on the mean optical depth are from Kim et al. (2007). For the temperature of the IGM, we follow Becker et al. (2011) and assume a future IGM study has determined γ to the required precision.

The effect of the primordial power spectrum evolves with redshift in a different way to T_0 and γ. Hence, sufficiently accurate data can break degeneracies between them. For τ_{eff}, the constraints from BOSS are already much tighter than our prior from Kim et al. (2007), so this prior provides no additional information. Overall, therefore, the extra information provided by our thermal priors has no significant effect on our reconstruction of the primordial power spectrum.

5 DISCUSSION

In this work, we have performed a minimally parametric reconstruction of the primordial power spectrum, using Lyman α data. This
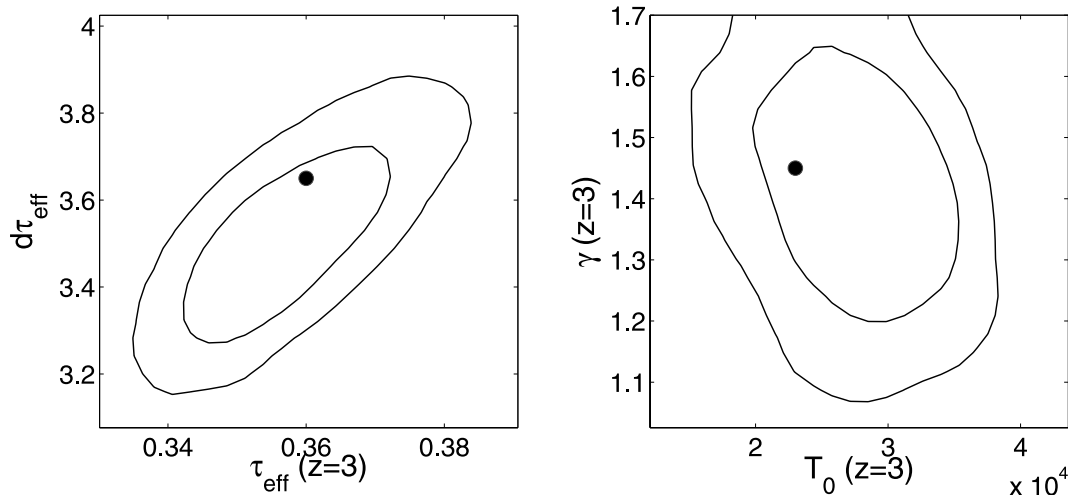
Figure 6. Joint 2D posterior constraints on the thermal history using forecast BOSS data. Input parameters are marked by black dots. Contours are drawn at 68 and 95 per cent CL. See Section 2.3 for definitions of the thermal parameters.

is an extension of McDonald et al. (2005b) and Viel & Haehnelt (2006), who used Lyman α data to measure the amplitude and slope of the primordial power spectrum on small scales, assuming that it had a power-law shape. Using a highly prescriptive model to fit data, even if it is physically motivated, can hide systematic effects, which may bias the recovered parameters in a manner which is hard to detect unless the bias is extremely large. Further, it is vital to go beyond parameter estimation and test the underlying model of the primordial power spectrum. This can in principle be achieved with a minimally parametric reconstruction framework coupled with a scheme for avoiding overfitting the data.

Peiris & Verde (2010), who attempted such a reconstruction including Lyman α data, assumed that the power spectrum could be well approximated by an amplitude, a power-law slope and its running across the scales probed by the Lyman α forest. In their analysis, this assumption was justified as the Lyman α data were treated as a single point and combined with CMB and galaxy survey data to reconstruct the power spectrum over a wide range of scales.

However, the only likelihood function available up to now contained a power-law assumption about the primordial power spectrum shape, making it impossible to treat the Lyman α data in a fully minimally parametric manner. We remedy this, performing a large suite of numerical simulations to construct a new likelihood function. The primordial power spectra thus emulated have considerable freedom in their shapes, specified by cubic smoothing splines. This provides the first ingredient for a minimally parametric reconstruction scheme.

The second ingredient, as mentioned above, is to avoid fitting the noise structure of the data with superfluous oscillations. To this end, our method uses CV to reconstruct the level of freedom allowed by the data. CV is a statistical technique which quantifies the notion that a good fit should be predictive. Schematically, it is a method of jack-knifing the data as a function of a 'roughness' penalty. A small penalty thus allows considerable oscillatory structure in the power spectrum shape, while a larger penalty specifies a smoother shape. This penalty term thus performs the same function as a prior on the smoothness of the power spectrum. Jackknifing the data then tests the predictivity of the smoothing prior, choosing as the optimal penalty the one that maximizes predictivity. For technical details see Section 2.1.

For the Lyman α current data from SDSS (McDonald et al. 2006), CV yields no significant preference for any particular penalty. In the context of CV, this indicates that no penalty is more predictive or favoured over any other; in other words, the data are not sufficiently powerful to accurately reconstruct the strength of the shape prior.

The minimally parametric method thus provides no evidence for features in the power spectrum in the current data, and our results are fully consistent with a scale-invariant power spectrum. The best-fitting amplitude of the power spectrum is, as in previous work, slightly higher than that extrapolated from *WMAP* (Komatsu et al. 2011). However, because the data do not contain sufficient statistical power to reconstruct the power spectrum shape, our error bars are extremely large. An analysis that uses different statistical techniques, such as Bayesian evidence (Jeffreys 1961), could provide further insight, but is beyond the scope of this paper.

In the not so distant future, the first data from a new Lyman α survey, BOSS (Schlegel et al. 2009), will be made available. We simulate a flux power spectrum and covariance matrix for BOSS, with an 80 fold increase in statistical power over the current data. In this case we successfully reconstruct the power spectrum, using CV to find an optimal penalty. The parameters we extract using CV are completely consistent with the inputs to the simulation, and the resulting constraints are comparable to those achieved by performing CV reconstruction using *WMAP* data (Verde & Peiris 2008). We verify that statistical error is the factor preventing us from finding an optimal penalty for current data by simulating a power spectrum identical to BOSS, but with wider error bars, again failing to find an optimal penalty.

Finally, we show that adding plausible future data on the small-scale thermodynamics of the IGM to BOSS does not significantly improve constraints on the primordial power spectrum. The simulated BOSS data are sufficiently powerful on their own to break degeneracies between the IGM and cosmological parameters, and are limited by statistical error rather than systematic uncertainty.

We have not considered the impact of the information BOSS is expected to provide on the transverse flux power spectrum. This will probe larger scales than our current work, offering a longer baseline and thus better sensitivity to the overall shape of the power spectrum.
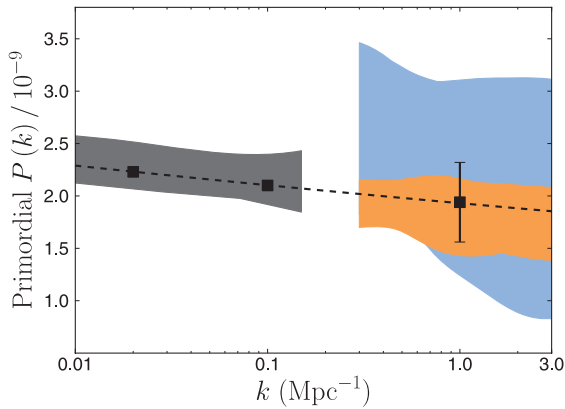
Figure 7. Comparison of our constraints. Blue is from current data; orange is our BOSS forecast. The grey region shows part of a reconstruction using both the CMB data and galaxy clustering measured by SDSS (Peiris & Verde 2010). The black squares show two knots used in the earlier reconstruction, while the black error bar shows 1σ constraints on power spectrum amplitude from parameter estimation (Viel et al. 2009). The dashed line shows the extrapolated *WMAP* best-fitting power spectrum.

However, applying the present technique to the improved data set would require simulations probing much larger scales, hence greatly increasing the numerical requirements.

Fig. 7 shows the constraints from BOSS in comparison to those of Peiris & Verde (2010) obtained by reconstructing the power spectrum using the CMB and the matter power spectrum from SDSS. By combining BOSS data with other probes (Seljak et al. 2005, 2006), such as galaxy clustering, the CMB and the transverse flux power spectrum, we will be able to accurately reconstruct the shape of the power spectrum on scales of $k = 0.001$–$3\,\mathrm{Mpc}^{-1}$, probing 10 e-folds of inflation.

REFERENCES

Becker G. D., Bolton J. S., Haehnelt M. G., Sargent W. L. W., 2011, MNRAS, 410, 1096
Bolton J. S., Becker G. D., 2009, MNRAS, 398, L26
Bolton J. S., Viel M., Kim T., Haehnelt M. G., Carswell R. F., 2008, MNRAS, 386, 1131
Carmack P. S., Schucany W. R., Spence J. S., Gunst R. F., Lin Q., Haley R. W., 2009, J. Comput. Graphical Statistics, 18, 879
Croft R. A. C., Weinberg D. H., Katz N., Hernquist L., 1998, ApJ, 495, 44
Gnedin N. Y., Hamilton A. J. S., 2002, MNRAS, 334, 107
Green P. J., Silverman B. W., 1994, Non-parametric Regression and Generalized Linear Models. Chapman and Hall, London
Haardt F., Madau P., 2001, in Neumann D. M., Tran J. T. V., eds, Clusters of Galaxies and the High Redshift Universe Observed in X-rays Modelling the UV/X-ray cosmic background with CUBA, CEA, Saclay, preprint (astro-ph/0106018)
Hui L., Burles S., Seljak U., Rutledge R. E., Magnier E., Tytler D., 2001, ApJ, 552, 15
Jeffreys H., 1961, Theory of Probability. Oxford Univ. Press, Oxford
Katz N., Weinberg D. H., Hernquist L., 1996, ApJS, 105, 19
Kim T., Bolton J. S., Viel M., Haehnelt M. G., Carswell R. F., 2007, MNRAS, 382, 1657
Komatsu E., Smith K., Dunkley J., Bennett C., Gold B. et al., 2011, ApJS, 192, 18
Lewis A., Bridle S., 2002, Phys. Rev. D, 66, 103511
Lewis A., Challinor A., Lasenby A., 2000, ApJ, 538, 473
Lidz A., Heitmann K., Hui L., Habib S., Rauch M., Sargent W. L. W., 2006, ApJ, 638, 27
McDonald P., 2003, ApJ, 585, 34
McDonald P., Eisenstein D. J., 2007, Phys. Rev. D, 76, 063009
McDonald P., Miralda Escudé J., Rauch M., Sargent W. L. W., Barlow T. A., Cen R., Ostriker J. P., 2000, ApJ, 543, 1
McDonald P., Seljak U., Cen R., Bode P., Ostriker J. P., 2005a, MNRAS, 360, 1471
McDonald P. et al., 2005b, ApJ, 635, 761
McDonald P. et al., 2006, ApJS, 163, 80
Meiksin A. A., 2009, Rev. Modern Phys., 81, 1405
Peiris H. V., Verde L., 2010, Phys. Rev. D, 81, 021302
Schaye J., Theuns T., Rauch M., Efstathiou G., Sargent W. L. W., 2000, MNRAS, 318, 817
Schlegel D., White M., Eisenstein D., 2009, Vol. 2010, in Astro2010: A&A Decadal Survey, The Baryon Oscillation Spectroscopic Survey: Precision measurement of the absolute cosmic distance scale. p. 314, preprint (arXiv:0902.4680)
Sealfon C., Verde L., Jimenez R., 2005, Phys. Rev. D, 72, 103520
Seljak U., Makarov A., McDonald P., Anderson S. F., Bahcall N. A. et al., 2005, Phys. Rev. D, 71, 103515
Seljak U., Slosar A., McDonald P., 2006, J. Cosmology Astropart. Phys., 10, 14
Slosar A., Ho S., White M., Louis T., 2009, J. Cosmology Astropart. Phys., 10, 19
Springel V., 2005, MNRAS, 364, 1105
Theuns T., Leonard A., Efstathiou G., Pearce F. R., Thomas P. A., 1998, MNRAS, 301, 478
Verde L., Peiris H. V., 2008, J. Cosmology Astropart. Phys., 0807, 009
Viel M., Haehnelt M. G., 2006, MNRAS, 365, 231
Viel M., Matarrese S., Mo H. J., Haehnelt M. G., Theuns T., 2002, MNRAS, 329, 848
Viel M., Haehnelt M. G., Springel V., 2004, MNRAS, 354, 684
Viel M., Bolton J. S., Haehnelt M. G., 2009, MNRAS, 399, L39
White M., Pope A., Carlson J., Heitmann K., Habib S., Fasel P., Daniel D., Lukic Z., 2010, ApJ, 713, 383

APPENDIX A: SIMULATED SPECTRA

In this appendix, we detail the procedure for extracting a spectrum from a simulation snapshot. First, we must find the velocity of each particle, including both peculiar velocities and the Hubble flow. The effect of peculiar velocities is to increase the flux power by around 10 per cent.

Next, we calculate the optical depth at wavelength λ, as defined by the line integral

$$\tau_\lambda = \int \sigma_\lambda n_{\mathrm{H}}\mathrm{d}l, \tag{A1}$$

where σ_λ is the cross-section for the transition and n_H is the number density of the neutral hydrogen. σ_λ is given by the rest cross-section multiplied by a broadening function

$$a_\lambda = \sigma_\alpha \times \Phi. \tag{A2}$$

We define the oscillator strength, f_α, by the ratio between the cross-section of the Lyman α transition and the cross-section of the transition involving a free electron

$$f_\alpha = \frac{\sigma_\alpha}{\pi r_0 \lambda}, \tag{A3}$$

where λ is the rest wavelength of the Lyman α transition. The classical radius of the electron, r_0, is related to the Thompson cross-section, σ_T, by

$$r_0 = \sqrt{\frac{3\sigma_T}{8\pi}}. \tag{A4}$$

Hence

$$\sigma_\alpha = \sqrt{\pi}\sqrt{\frac{3\sigma_T}{8}} f_\alpha \lambda. \tag{A5}$$

To compute the broadening function, we neglect natural broadening from the intrinsic uncertainty in the energy levels of the hydrogen atom. Natural broadening is only important in the densest absorbers (damped Lyman α systems), which our simulations lack the resolution to adequately resolve. The effect of DLAs is included by a correction applied when calculating the likelihood, for which see Section 2.6.2.

Hence the only form of broadening present is Doppler broadening. In an absorber of temperature T_H, mass m_H and velocity v, the probability of a particle having zero velocity relative to an incoming photon is

$$\Phi = \frac{c}{\sqrt{\pi}b} \exp\left[-\frac{v^2}{b}\right],$$
$$\text{where } b = \sqrt{\frac{2kT_H}{m_H}}. \tag{A6}$$

Hence, a wavelength bin at position k will suffer absorption from a HI absorber in a bin j as

$$\tau_{kj} = \sigma_\alpha \Phi n_H a \Delta \tag{A7}$$

$$= \sigma_\alpha \frac{c}{\sqrt{\pi}b} n_H a \Delta \exp\left[-\left(\frac{v_k - v_j}{b}\right)^2\right]. \tag{A8}$$

Here Δ is the bin width, and a is the expansion factor.

The flux in each bin is then simply $\mathcal{F} = e^{-\tau}$. Each spectrum is smoothed with a simple three-point boxcar average, following Viel et al. (2004), and the flux power spectrum from the simulation box is defined to be the average over a number of simulated spectra.

APPENDIX B: CONVERGENCE CHECKS

In this appendix, we detail the checks we have performed to ensure that our simulations are properly converged with respect to box size and particle number. We have usually been comparing the relative change in the flux power spectrum when changing a parameter, making strict convergence not essential.

To check box-size convergence, we compared the flux $P_F(k)$ for our fiducial simulation with a large box-size simulation ('L') which had size (75, 500), and otherwise identical parameters to the fiducial simulation ('F'). This isolates the effect of box size by having identical particle resolution to simulation F. To test convergence with respect to particle number, we used a high-resolution simulation ('H'), with (60, 500). In order to isolate the change due to numerical effects, we did not rescale the mean optical depth for the plots in this section.

The left-hand plot of Fig. B1 shows the change in the flux power spectrum with increased box size; simulation L divided by simulation F. The flux power spectrum is converged with respect to box size; however, there is a systematic increase on large scales. This is due to sample variance: the specific realization of cosmic structure we are using is biased slightly low on the largest scales probed by the box. The larger box recovers the input power spectrum much better on these scales, because it contains far more modes, and hence shows an increase in power. Because we use the same realization of structure for all our simulations, this effect will be constant and is easily corrected for by altering the best-fitting power spectrum. Once this is done, convergence of the flux power spectrum is very good.

The right-hand plot of Fig. B1 shows the change in the flux power spectrum with increased particle resolution. The effect is small, except on small scales or at high redshift. Achieving numerical convergence for the Lyman α forest at high redshift is challenging, because most of the signal for the Lyman α forest is coming from poorly resolved underdense regions. In addition, current data at high
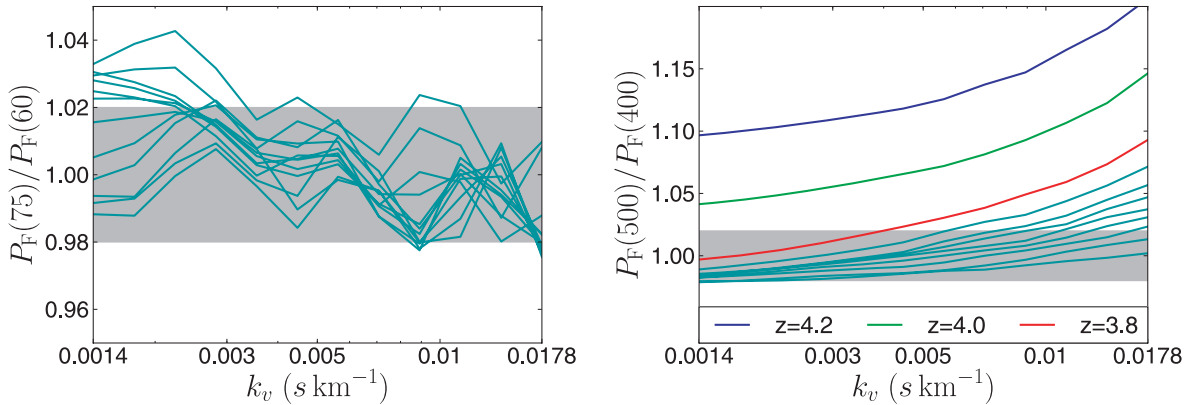

Figure B1. Left: the change in the flux power spectrum due to increasing the box size at fixed particle resolution. Each green line shows the effect on a different redshift bin, from 4.2 to 2.0. The effect is generally around 2 per cent (grey box), with a systematic increase on large scales, for which we correct (see text). Right: the effect on the flux power spectrum due to increasing the particle number from 2×400^3 to 2×500^3. Each line shows the effect on a different redshift bin, from 4.2 to 2.0. The grey box show a variation of 4 per cent. Redshift bins with greater variation are labelled.

redshifts are much more noisy than at low redshifts, due to a paucity of quasar spectra. Accordingly, we follow Viel & Haehnelt (2006) and do not use the three highest redshift bins at $z = 4.2, 4.0$ and 3.8 in our analysis.

Our initial base for the central power spectrum was the output of simulation H. We corrected for box size and resolution following the method proposed by McDonald (2003). To correct for sample variance on the largest scales, we ran two additional simulations with box size $120 \, \mathrm{Mpc} \, h^{-1}$, and 400^3 and 200^3 particles. The smaller simulation has identical particle resolution to our fiducial simulations, and should thus be directly comparable to them. We then corrected our best-guess power spectrum by the ratio between the two:

$$C_S(k) = P_\mathrm{F}(N_P = 400)/P_\mathrm{F}(N_P = 200). \tag{B1}$$

The smallest scale bin was excluded from this correction as it was clearly being affected by poor resolution convergence.

Because simulation H is nearly converged, we had to be careful when correcting for resolution; if the error in the correction is larger than the correction itself, accuracy is definitely not increased. Therefore, we ran two simulations, with box size of $24 \, \mathrm{Mpc} \, h^{-1}$; $T1$ and $T2$. $T1$ has the same particle resolution as simulation H, and thus 200^3 particles. $T2$ has 400^3, giving it much increased particle resolution. These simulations do not resolve the largest scales probed by the Lyman α forest at all, but Fig. B1 shows that these scales are not affected by poor resolution convergence. Simulation H is corrected by

$$C_R(k) = P_\mathrm{F}^{T2} \big/ P_\mathrm{F}^{T1}. \tag{B2}$$

To avoid our correction itself being biased by a small box size, we ignore those bins on scales greater than a quarter of the box size of $24 \, \mathrm{Mpc} \, h^{-1}$. We also ignore any correction for redshift bins where the correction for the smallest scale bin is less than the uncertainty in the simulations, which we take to be 1 per cent, on the grounds that these are already fully converged. We are left with a slight increase in power on the smallest scales.

This paper has been typeset from a TEX/LATEX file prepared by the author.